eprints@whiterose.ac.uk
https://eprints.whiterose.ac.uk/

SRF-based current-limiting droop controller for three-phase grid-tied inverters

Alexandros G. Paspatis and George C. Konstantopoulos

Dept. Automatic Control and Systems Engineering
The University of Sheffield
Sheffield, UK

{apaspatis1, g.konstantopoulos}@sheffield.ac.uk

Abstract—A nonlinear droop controller for three-phase grid-connected inverters that guarantees a rigorous current limitation and asymptotic stability for the closed-loop system is proposed in this paper. The proposed controller is designed using the synchronous reference frame (SRF) and can easily change its operation between the PQ-set mode, i.e. accurate regulation of real and reactive power to their reference values, and the droop control mode. Furthermore, nonlinear input-to-state stability theory is used to guarantee that the grid current remains limited below a given value under both normal and abnormal grid conditions (grid faults). Asymptotic stability for any equilibrium point of the closed-loop system is also analytically proven. The proposed control approach is verified through extended real-time simulation results of a three-phase inverter connected to both a normal and a faulty grid.

Index Terms—Nonlinear control, three-phase inverter, synchronous reference framework, droop control, stability analysis.

I. INTRODUCTION

IN order to accomplish large-scale utilization of distributed energy resources (DERs) in the modern smart grid architecture, all stringent requirements imposed by the Grid Code are needed to be fulfilled by every grid-connected DER unit [1]. Since the integration of DERs is achieved via power inverters, advanced control techniques are required for grid-connected inverters to guarantee a stable, reliable and resilient power network.

The control of the power electronic interfaced DERs connected to the main grid or a microgrid represents an active topic and among different control approaches, droop control represents the most widely used control technique for DERs since it has the ability to regulate to grid voltage and frequency [2]. In this context, enhanced droop controllers have been proposed with improved stability properties by either mimicking the frequency inertia of the conventional synchronous generators [3], [4], [5], [6] or by introducing robust control methods for better voltage and frequency regulation and increased protection [7], [8]. These droop control approaches are mostly implemented in a multi-loop structure with inner current and voltage control loops and the outer power loop (droop control) to improve the power quality [9]. A number of recent works has also emphasized on the importance of combining droop control with a virtual output impedance, e.g. resistive or inductive, of the power electronic devices to further enhance closed-loop system stability [10], [11]. However, since different output impedances lead to different droop expressions, a universal droop controller that introduces the same structure regardless of the output impedance has been recently proposed in [2].

Although grid support is a key property for grid-connected inverters and can be achieved via the droop control, the protection of the power inverter units and the interconnected DER is also of major significance. Since overcurrents resulting from sudden grid voltage drops can harm the inverter units, current-limiting techniques should be embedded into the control design of every inverter-interfaced DER unit [12], [13]. In voltage-controlled inverters, the current-limitation is mainly accomplished through saturated integrators in the inner loops, which may suffer from integrator wind-up and eventually lead to instability [14], or by switching to a different current-limiting controller when an abnormal grid condition is identified. However, such a switching operation can still suffer from integrator wind-up or force the controller to latch-up [15], [16], [17]. In order to overcome these instability issues and achieve the desired current limitation for grid-connected inverters, the virtual impedance or resistance concept offers a promising solution [14], [18]. To this end, a new current-limiting droop control concept has been proposed in [19] for single-phase inverters where no switching actions or saturated integrators are used for the current limitation. However, this approach cannot be directly applied to three-phase inverters, especially using the widely adopted $dq0$ synchronous reference frame (SRF) for the modeling of the inverter and the control design. Furthermore, the asymptotic stability of any equilibrium point of the closed-loop system using the current-limiting droop control of [19] is still left to be proven. Even though the well-known small-signal stability analysis is still extensively used today [20], [2], the stability analysis of droop-controlled inverters without assuming knowledge of the system parameters still represents a challenging task.

In this paper, a current-limiting droop control of three-phase inverters connected to the grid via an LCL filter and modeled in the synchronous reference frame is proposed. Compared to the natural framework (NF, abc) used for example in [19] and
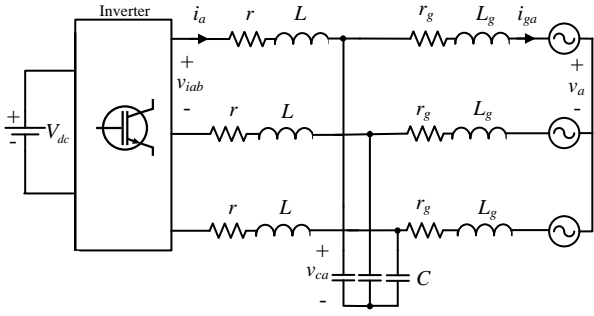
Figure 1. Three-phase inverter connected to the grid through an LCL filter

the stationary framework (SF, $\alpha\beta0$) in [21], the SRF has the advantage that transforms the ac quantities to dc at the steady state and thus conventional regulating controllers can be used. The proposed control approach enables the inverter to either track the set reference values for the real and reactive power or to operate with a droop control technique to support the grid. Furthermore, a grid current-limiting property is shown to be sustained at all times by introducing a virtual resistance and is analytically proven using the input-to-state stability (ISS) property of the closed-loop system. This current-limitation ensures a safe operation even in the case where voltage dips occur in the grid without the need of saturation units that can lead to instability. Finally, asymptotic stability for the closed-loop system is also proven without assuming knowledge of the system parameters. The proposed control approach is verified through extended real-time simulation results under both normal and abnormal grid conditions.

The paper is organized as follows. In Section II, the dynamic model of the three-phase inverter in the SRF is provided and the research problem is stated. In Section III, the proposed control approach is analytically presented. In Section IV, the current-limiting property of the proposed controller is mathematically proven and the asymptotic stability of the closed-loop system is analytically shown. In Section V, real-time simulation results are shown to validate the control approach and in Section VI, the derived conclusions are given.

II. SYSTEM MODELING AND PROBLEM FORMULATION

The system under consideration consists of a three-phase inverter connected to the grid through an LCL filter, as depicted in Fig. 1. The capacitors of the filter are denoted as C, while the inductances are denoted as L and L_g with parasitic resistances r and r_g, respectively. The line-to-line voltage between phases a and b is given as v_{iab}, while v_{ia} represents the phase voltage of the inverter. The capacitor voltage is denoted as v_{ca} and the grid voltage is v_a with $v_a = \sqrt{2}V_g \sin\omega_g t$, where V_g is the RMS grid voltage and ω_g is the angular grid frequency. The inverter and grid side currents are i_a and i_{ga} respectively. In order to obtain the dynamic model of the system, the widely used SRF theory is considered [22].

Although the clockwise SRF transformation from [23] is most commonly used with phase a aligned to the α axis, in

this paper the generic $\alpha\beta$ transformation is taken into account as presented in [24]:

$$T_{\alpha\beta} = \frac{2}{3} \begin{bmatrix} cos\theta_a & cos(\theta_a - 120^o) & cos(\theta_a + 120^o) \\ sin\theta_a & sin(\theta_a - 120^o) & sin(\theta_a + 120^o) \\ 0.5 & 0.5 & 0.5 \end{bmatrix},$$

where θ_a is the angle between phase a and the α axis, followed by the rotating transformation

$$T_{dq} = \begin{bmatrix} cos\theta_g & -sin\theta_g \\ sin\theta_g & cos\theta_g \end{bmatrix},$$

with $\theta_g = \omega_g t$.

By applying the above transformations to the three-phase current and voltage quantities of the system, the SRF-based dynamic equations of the three-phase grid-tied inverter are obtained as

$$L\frac{di_d}{dt} = v_{id} - v_{cd} - ri_d - \omega_g L i_q \tag{1}$$

$$L\frac{di_q}{dt} = v_{iq} - v_{cq} - ri_q + \omega_g L i_d \tag{2}$$

$$L_g\frac{di_{gd}}{dt} = v_{cd} - v_d - r_g i_{gd} - \omega_g L_g i_{gq} \tag{3}$$

$$L_g\frac{di_{gq}}{dt} = v_{cq} - v_q - r_g i_{gq} + \omega_g L_g i_{gd} \tag{4}$$

$$C\frac{dv_{cd}}{dt} = i_d - i_{gd} - \omega_g C v_{cq} \tag{5}$$

$$C\frac{dv_{cq}}{dt} = i_q - i_{gq} + \omega_g C v_{cd}, \tag{6}$$

where v_{id} and v_{iq} are the dq-axis values of the inverter voltage and represent the control inputs of the system [25].

The aim of the inverter is to operate using droop control, which represents the most commonly used approach for power electronics interfaced DERs to mimic the dynamic response of synchronous generators and support the grid voltage and frequency. Since the inverter is required to operate in a unified way under both normal and abnormal conditions, in [19], a novel current-limiting technique has been proposed for droop controlled single-phase grid-connected inverters. However, in order to extend this technique to three-phase inverters, the current-limiting droop control should be designed in SRF instead of NF to reduce the computational burden and facilitate the use of regulating control schemes. This design also allows the investigation of the asymptotic stability of the closed-loop system. Furthermore, in order to achieve better power quality, the multi-loop control strategy is adopted, as explained in [9]. Therefore, a new droop control structure for three-phase inverters that guarantees a limit for the grid current and asymptotic stability using a multi-loop control strategy is proposed in the sequel.

III. THE PROPOSED CONTROLLER

The proposed controller consists of an inner-loop voltage and current controller and an outer-loop power controller, which includes the droop control characteristics and inherently limits the grid current.

A. Inner-loop controller

The inner-loop current controller takes the form

$$v_{id} = v_{cd} + \left(k_{PCC} + \frac{k_{ICC}}{s} \right) (i_d^{ref} - i_d) + \omega_g L i_q$$

$$v_{iq} = v_{cq} + \left(k_{PCC} + \frac{k_{ICC}}{s} \right) (i_q^{ref} - i_q) - \omega_g L i_d$$

where PI controllers with decoupling terms are applied to regulate i_d to i_d^{ref} and i_q to i_q^{ref}. Similarly, the voltage controller from which i_d^{ref} and i_q^{ref} are obtained is described through the equations

$$i_d^{ref} = i_{gd} + \left(k_{PVC} + \frac{k_{IVC}}{s} \right) (v_{cd}^{ref} - v_{cd}) + \omega_g C v_{cq}$$

$$i_q^{ref} = i_{gq} + \left(k_{PVC} + \frac{k_{IVC}}{s} \right) (v_{cq}^{ref} - v_{cq}) - \omega_g C v_{cd}$$

where the reference values v_{cd}^{ref} and v_{cq}^{ref} are defined by the outer-loop power control.

As in typical multi-loop controller applications, the current controller is designed to settle much faster than the voltage controller which settles much faster than the power controller. In order to satisfy this, the parameters of the PI controllers can be suitably selected using the pole placement technique. Thus, for the power controller design, which operates in a slower time scale, it is reasonable to assume that v_{cd} and v_{cq} are quickly regulated to v_{cd}^{ref} and v_{cq}^{ref}. Further analysis about the inner-loop controllers commonly used in DERs applications can be found in [26].

B. The proposed droop controller

The outer-loop controller consists of a power controller which adopts droop control to support the grid. Following the introduction of the inner-loop controller in the previous subsection, the power controller will be directly applied to the capacitor voltage of the LCL filter through controlling the reference capacitor voltage values v_{cd}^{ref} and v_{cq}^{ref}. The proposed power controller for the grid-connected operation is described by the equations

$$v_{cd}^{ref} = v_d + E_d^* - w_d i_{gd} + \omega_g L_g i_{gq} \qquad (7)$$

$$v_{cq}^{ref} = v_q + E_q^* - w_q i_{gq} - \omega_g L_g i_{gd} \qquad (8)$$

where w_d, w_q are the virtual resistances applied to each axis and which change according to the expressions

$$\dot{w_d} = -c_{wd} f(P) w_{dq}^2 \qquad (9)$$

$$\dot{w_{dq}} = \frac{c_{wd}(w_d - w_m)w_{dq}}{\Delta w_m^2} f(P) - k_w \left(\frac{(w_d - w_m)^2}{\Delta w_m^2} + w_{dq}^2 - 1 \right) w_{dq}$$

$$\dot{w_q} = -c_{wq} g(Q) w_{qq}^2 \qquad (10)$$

$$\dot{w_{qq}} = \frac{c_{wq}(w_q - w_m)w_{qq}}{\Delta w_m^2} g(Q) - k_w \left(\frac{(w_q - w_m)^2}{\Delta w_m^2} + w_{qq}^2 - 1 \right) w_{qq}$$

where $c_{wd}, c_{wq}, k_w, w_m, \Delta w_m$ are positive constants and

$$f(P) = n(P_{set} - P) + K_e \left(E_{rms}^* - V_g \right) \qquad (11)$$

$$g(Q) = m(Q_{set} - Q) - (\omega^* - \omega_g) \qquad (12)$$
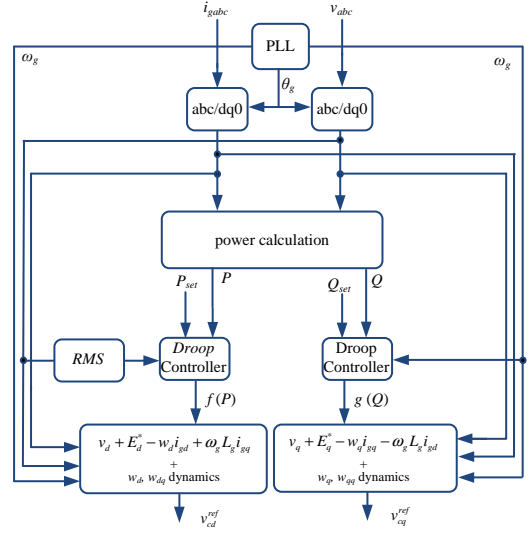
Figure 2. Implementation of the proposed power controller

with E_d^* and E_q^* representing the nominal voltages on dq axes, K_e being a positive constant, E_{rms}^* is the RMS nominal voltage and m, n are the droop coefficients. The real and reactive power of the inverter are denoted as P and Q with their desired values P_{set} and Q_{set}, respectively. It should be highlighted that due to the virtual resistances w_d and w_q introduced by the proposed controller, the $P \sim V$ and $Q \sim -\omega$ droop expressions are adopted here (for details see [19]).

The PQ-set and PQ-droop control modes can be also implemented in the control system through the functions (11)-(12). In these two control modes, the inverter is either tracking the reference values P_{set}, Q_{set}, when the terms $K_e \left(E_{rms}^* - V_g \right)$ and $\omega^* - \omega_g$ are removed from (11) and (12), respectively, or regulates to the grid voltage and frequency to support the grid. For the dynamics of the virtual resistances w_d and w_q in (7)-(8), the bounded integral controller, proposed in [27], is adopted in order to guarantee the boundedness of w_d and w_q without using any saturated integrators that could drive the system to instability. Hence, it is guaranteed that $w_d, w_q \in [w_{min}, w_{max}] > 0$, for all $t \geq 0$, where $\Delta w_m = \frac{w_{max} - w_{min}}{2}$ and $w_m = \frac{w_{min} + w_{max}}{2}$. For more details, the reader is referred to [27]. This design of bounded virtual resistance will lead to the desired current-limiting property as explained in the sequel. The implementation of the proposed control approach is depicted in Fig. 2.

IV. STABILITY ANALYSIS

A. Current-limiting property

By substituting the proposed controller equations (7) and (8) into the system dynamics (3)-(4), and taking into account the fast inner current and voltage control loops that regulate v_{cd} and v_{cq} to v_{cd}^{ref} and v_{cq}^{ref} in (3) and (4), the closed-loop system can be obtained as:

$$L_g \frac{di_{gd}}{dt} = E_d^* - w_d i_{gd} - r_g i_{gd} \qquad (13)$$

$$L_g \frac{di_{gq}}{dt} = E_q^* - w_q i_{gq} - r_g i_{gq}. \qquad (14)$$

The equations (13) and (14) are the derived dynamics of the grid current. Recall that for the controller dynamics w_d, w_{dq}, w_q, w_{qq} it holds true that $w_d, w_q \in [w_{min}, w_{max}] > 0$, where $w_{min} = w_m - \Delta w_m$, $w_{max} = w_m + \Delta w_m$, for all $t \geq 0$. Taking into account these properties, let us consider the Lyapunov function candidate

$$V = \frac{1}{2} L_g i_{gd}^2 + \frac{1}{2} L_g i_{gq}^2.$$

The time derivative of V, after substituting into its expression the dynamic equation of the grid current, becomes

$$\dot{V} = -r_g(i_{gd}^2 + i_{gq}^2) + \left(i_{gd}(E_d^* - w_d i_{gd}) + i_{gq}(E_q^* - w_q i_{gq})\right)$$

$$\leq -(r_g + w_{min})(i_{gd}^2 + i_{gq}^2) + \begin{bmatrix} E_d^* & E_q^* \end{bmatrix} \begin{bmatrix} i_{gd} \\ i_{gq} \end{bmatrix}$$

$$\leq -(r_g + w_{min}) \|i_g\|_2^2 + \|E^*\|_2 \|i_g\|_2,$$

where $i_g = \begin{bmatrix} i_{gd} & i_{gq} \end{bmatrix}^T$ and $E^* = \begin{bmatrix} E_d^* & E_q^* \end{bmatrix}^T$. Hence,

$$\dot{V} < 0, \forall \|i_g\|_2 > \frac{\|E^*\|_2}{(r_g + w_{min})},$$

which means that the grid current dynamics system given by equations (13) and (14) is input-to-state stable (ISS) when the voltage vector E^* is considered as input. Since E_d^* and E_q^* represent constant values of the rated voltage then the grid currents i_{gd} and i_{gq} will be bounded for all $t \geq 0$.

Since $i_g = \begin{bmatrix} i_{gd} & i_{gq} \end{bmatrix}^T$ and $E^* = \begin{bmatrix} E_d^* & E_q^* \end{bmatrix}^T$ and if we consider the relationship between the RMS value and the dq components, then

$$\|i_g\|_2 = \sqrt{i_{gd}^2 + i_{gq}^2} = \sqrt{(\sqrt{2} I_{grms})^2} = \sqrt{2} I_{grms}$$

$$\|E^*\|_2 = \sqrt{E_d^{*2} + E_q^{*2}} = \sqrt{(\sqrt{2} E_{rms}^*)^2} = \sqrt{2} E_{rms}^*.$$

Given a maximum RMS value of the grid current I_{grms}^{max}, then by selecting the controller parameter $w_{min} = \frac{E_{rms}^*}{I_{grms}^{max}}$ and taking into account that the system (13)-(14) is ISS, it holds true that if at the time that the controller is enabled, the grid current is less than the maximum I_{grms}^{max}, i.e. $I_{grms}(0) < I_{grms}^{max}$, then

$$I_{grms}(t) \leq \frac{E_{rms}^*}{(r_g + w_{min})} = \frac{I_{grms}^{max}}{\frac{I_{grms}^{max} r_g}{E_{rms}^*} + 1} < I_{grms}^{max}, \forall t > 0.$$

Hence, it is mathematically proven that the grid current of the inverter will never violate a given maximum value I_{grms}^{max} via the control design. It is highlighted that the maximum value of the grid current is guaranteed by suitably selecting the minimum value of the virtual resistances w_d and w_q in the proposed controller dynamics.
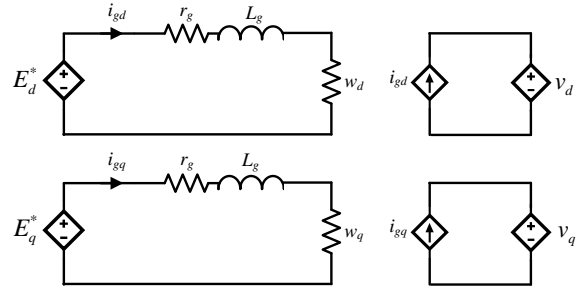

Figure 3. The equivalent closed-loop system

B. Asymptotic Stability

As it can be seen from (13)-(14), the dynamics of the grid current are decoupled from the inverter current and capacitor voltage dynamics and are independent from each other due to the lack of cross-coupling terms. The equivalent circuit of the three-phase grid-connected inverter can be simplified as shown in Fig. 3 and its dynamics are given by (13)-(14) and (9)-(12). Given that in the used SRF the real and reactive power can be calculated from $P = \frac{3}{2}(v_d i_{gd} + v_q i_{gq})$ and $Q = \frac{3}{2}(v_d i_{gq} - v_q i_{gd})$, the state vector of the closed-loop system is $x = [w_d \; w_{dq} \; w_q \; w_{qq} \; i_{gd} \; i_{gq}]^T$. Since $w_d, w_q \in [w_{min}, w_{max}]$ then for any equilibrium point $x_e = [w_{de} \; w_{dqe} \; w_{qe} \; w_{qqe} \; i_{gde} \; i_{gqe}]^T$, with $w_{dqe}, w_{qqe} \in (0, 1]$, the investigation of closed-loop system stability using the Jacobian matrix results into two negative eigenvalues $-2k_w w_{dqe}^2$ and $-2k_w w_{qqe}^2$ and the remaining eigenvalues obtained from matrix

$$A = \begin{bmatrix} 0 & 0 & c_{wd} w_{dqe}^2 n \frac{3}{2} v_d & c_{wd} w_{dqe}^2 n \frac{3}{2} v_q \\ 0 & 0 & -c_{wq} m w_{qqe}^2 \frac{3}{2} v_q & c_{wq} w_{qqe}^2 m v_d \frac{3}{2} \\ -\frac{E_d^*}{L_g(r_g + w_{de})} & 0 & -\frac{w_{de} + r_g}{L_g} & 0 \\ 0 & -\frac{E_q^*}{L_g(r_g + w_{qe})} & 0 & -\frac{w_{qe} + r_g}{L_g} \end{bmatrix}.$$

To ensure the asymptotic stability, the eigenvalues of A need to have negative real parts. The characteristic polynomial of matrix A is $\lambda^4 + \alpha_3 \lambda^3 + \alpha_2 \lambda^2 + \alpha_1 \lambda + \alpha_0 = 0$, where

$$\alpha_3 = \frac{w_{de} + w_{qe} + 2r_g}{L_g}$$

$$\alpha_2 = \beta \frac{E_{rms}^*}{L_g(r_g + w_{de})} + \alpha \frac{E_{rms}^*}{L_g(r_g + w_{qe})} + \frac{(w_{de} + r_g)(w_{qe} + r_g)}{L_g^2}$$

$$\alpha_1 = \alpha \frac{E_{rms}^*(w_{de} + r_g)}{L_g^2(w_{qe} + r_g)} + \beta \frac{E_{rms}^*(w_{qe} + r_g)}{L_g^2(w_{de} + r_g)}$$

$$\alpha_0 = \frac{2\alpha\beta E_{rms}^{*2}}{L_g^2(w_{de} + r_g)(w_{qe} + r_g)}$$

with $\alpha = c_{wq} w_{qqe}^2 m \frac{3}{2} V_g$ and $\beta = c_{wd} w_{dqe}^2 n \frac{3}{2} V_g$, where $V_g = v_d = v_q$ and $E_{rms}^* = E_d^* = E_q^*$. Note that $v_d = v_q$ and $E_d^* = E_q^*$ can be achieved by selecting $\theta_a = 45^o$ in the generic $T_{\alpha\beta}$ transformation. To ensure the asymptotic stability of x_e, then using the Ruth-Hurwitz criterion, the following condition needs to be satisfied

$$(w_{de} + r_g)^2 (w_{qe} + r_g)^2 > (\alpha + \beta) E_{rms}^* L_g. \quad (15)$$

By selecting the controller gains $c_{wq} = \frac{\gamma c}{m}$ and $c_{wd} = \frac{c}{n}$, where γ is a gain coefficient to ensure the appropriate settling time difference between w_d and w_q dynamics, and taking into

account that $w_{de}, w_{qe} > w_{min} = \frac{E^*_{rms}}{I^{max}_{grms}}$, then the condition to guarantee asymptotic stability results in

$$c < \frac{2\left(\frac{E^*_{rms}}{I^{max}_{grms}} + r_g\right)^4}{3V_g E^*_{rms} L_g(\gamma + 1)}. \tag{16}$$

According to (16), the controller parameter c can be selected accordingly to guarantee asymptotic stability for any equilibrium point x_e in addition to the desired current-limiting property.

Table I
SYSTEM AND CONTROLLER PARAMETERS

Parameters	Values	Parameters	Values
L, L_g	2.2 mH	K_e	1
r, r_g	1 Ω	ω_g	2π x 49.98 rad/s
C	1 μF	I^{max}_{grms}	3 A
E^*_{rms}	110 V	w_m	294.4Ω
c_{wd}	380	Δw_m	257.8 Ω
c_{wq}	6664	k_w	1000
n	0.0056	m	0.0032

V. REAL-TIME SIMULATION RESULTS

In order to verify the proposed control approach, a three-phase grid-connected inverter equipped with the controller proposed in Section III is tested using the OP4500 OPAL-RT real-time digital simulator. The parameters of the controller and the system are given in Table I. The controller is enabled and the reference values P_{set} and Q_{set} initially have the values of 400 W and 0 Var, respectively. The proposed controller operates initially in the PQ-set mode and regulates P and Q to their desired values, as shown in Figures 4a and 4b. In Fig. 4d, one can observe that the voltage remains at its nominal value during this operation since a stiff grid is assumed. At 5s, Q_{set} is changed to 50 Var and the reactive power injection is accordingly modified, as depicted in Fig. 4b, while at 10s, P_{set} is set as 600 W. At 15s, the droop control operation is enabled and both the real and reactive power drop due to the slightly higher value of the grid voltage compared to the nominal (110.3 V) and the slightly lower than the nominal grid frequency (49.98 Hz). At 20s, a grid voltage drop of 0.2 p.u. occurs (as shown in Fig. 4d) to test the operation under faults and the desired current-limiting property of the controller. As shown in Fig. 4c, the grid current reaches its maximum RMS value of 3 A, as it has been analytically proven in this paper, thus protecting the inverter under grid faults. When the fault is self-cleared at 25s, P and Q return to their original values according to droop control, always without violating the maximum grid current.

Regarding the controller states introduced in the control design, one can observe in Figures 5a and 5b the time response of w_d and w_q in order to regulate the real and reactive power accordingly. As observed in Fig. 5a, when the current limit is triggered at 20s, w_d reaches its minimum value ($w_{min} = \frac{E^*_{rms}}{I^{max}_{grms}} = \frac{110}{3} = 36.66\Omega$) in order to maintain the grid current limited below its given maximum value.

VI. CONCLUSIONS

In this paper, a new droop controller for three-phase grid-connected inverters introduced in a multi-loop structure based
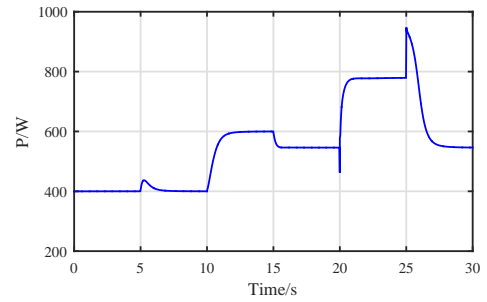
(a) Real Power
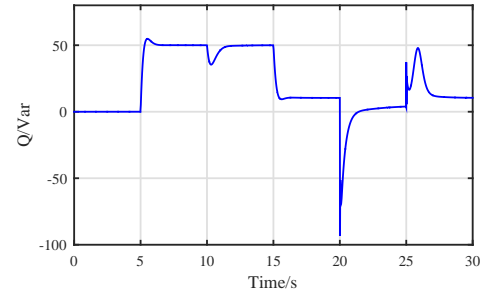
(b) Reactive power
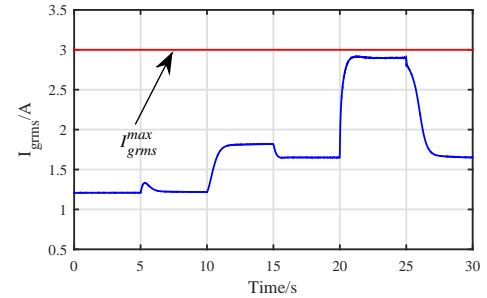
(c) RMS grid current
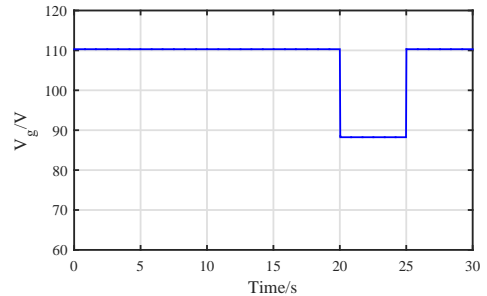

(d) RMS Voltage

Figure 4. Response of the three-phase grid-connected inverter equipped with the proposed controller

on SRF modeling was presented. The proposed controller was proven to inherit a current-limiting property for the grid-side inverter current and guarantee asymptotic stability for the closed-loop system. The proposed design enables a simple switch between PQ-set and PQ-droop control modes to either control the injected real and reactive power to set reference values or support the grid. Using nonlinear ISS theory of the closed-loop system, it was shown that the desired grid current limitation is maintained even when faults occur at
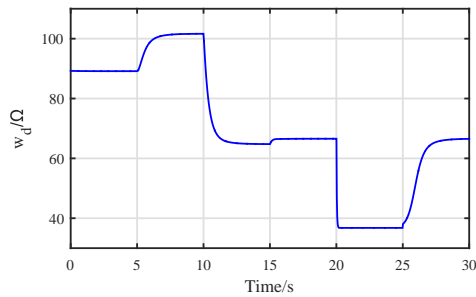
(a) Time response of the controller state w_d
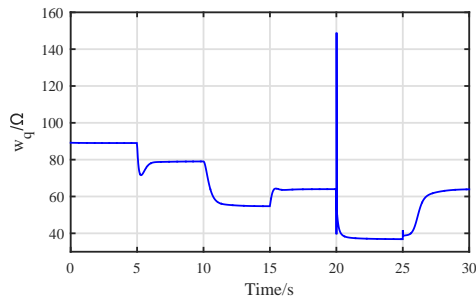
(b) Time response of the controller state w_q

Figure 5. Time response of the proposed controller states

the grid voltage, offering a unified control structure for both normal and abnormal grid condition. The effectiveness of the proposed control approach was verified through extended real-time simulation results both under a normal and a faulty grid.

REFERENCES

[1] Q. C. Zhong, "Power-electronics-enabled autonomous power systems: Architecture and technical routes," *IEEE Transactions on Industrial Electronics*, vol. 64, no. 7, pp. 5907–5918, July 2017.

[2] Q. C. Zhong and Y. Zeng, "Universal droop control of inverters with different types of output impedance," *IEEE Access*, vol. 4, pp. 702–712, 2016.

[3] Q.-C. Zhong and T. Hornik, *Synchronverters: Grid-Friendly Inverters That Mimic Synchronous Generators*. Wiley-IEEE Press, 2012, pp. 277–296.

[4] A. G. Paspatis and G. C. Konstantopoulos, "Current-limiting droop control with virtual inertia and self-synchronization properties," in *IECON 2017 - 43rd Annual Conference of the IEEE Industrial Electronics Society*, Oct 2017, pp. 196–201.

[5] J. Alipoor, Y. Miura, and T. Ise, "Power system stabilization using virtual synchronous generator with alternating moment of inertia," *IEEE Journal of Emerging and Selected Topics in Power Electronics*, vol. 3, no. 2, pp. 451–458, 2015.

[6] J. Liu, Y. Miura, and T. Ise, "Comparison of dynamic characteristics between virtual synchronous generator and droop control in inverter-based distributed generators," *IEEE Trans. Power Electron.*, vol. 31, no. 5, pp. 3600–3611, 2016.

[7] Y. Deng, Y. Tao, G. Chen, G. Li, and X. He, "Enhanced power flow control for grid-connected droop-controlled inverters with improved stability," *IEEE Transactions on Industrial Electronics*, vol. 64, no. 7, pp. 5919–5929, July 2017.

[8] X. Zhao, J. M. Guerrero, M. Savaghebi, J. C. Vasquez, X. Wu, and K. Sun, "Low-voltage ride-through operation of power converters in grid-interactive microgrids by using negative-sequence droop control," *IEEE Transactions on Power Electronics*, vol. 32, no. 4, pp. 3128–3142, April 2017.

[9] L. Huang, H. Xin, Z. Wang, K. Wu, H. Wang, J. Hu, and C. Lu, "A virtual synchronous control for voltage-source converters utilizing dynamics of dc-link capacitor to realize self-synchronization," *IEEE Journal of Emerging and Selected Topics in Power Electronics*, vol. 5, no. 4, pp. 1565–1577, Dec 2017.

[10] J. M. Guerrero, L. G. de Vicuna, J. Matas, M. Castilla, and J. Miret, "Output impedance design of parallel-connected ups inverters with wireless load-sharing control," *IEEE Transactions on Industrial Electronics*, vol. 52, no. 4, pp. 1126–1135, Aug 2005.

[11] J. M. Guerrero, J. Matas, L. G. de Vicuna, M. Castilla, and J. Miret, "Decentralized control for parallel operation of distributed generation inverters using resistive output impedance," *IEEE Transactions on Industrial Electronics*, vol. 54, no. 2, pp. 994–1004, April 2007.

[12] A. Camacho, M. Castilla, J. Miret, A. Borrell, and L. G. de Vicuna, "Active and reactive power strategies with peak current limitation for distributed generation inverters during unbalanced grid faults," *IEEE Transactions on Industrial Electronics*, vol. 62, no. 3, pp. 1515–1525, March 2015.

[13] H. Xin, L. Huang, L. Zhang, Z. Wang, and J. Hu, "Synchronous instability mechanism of p-f droop-controlled voltage source converter caused by current saturation," *IEEE Transactions on Power Systems*, vol. 31, no. 6, pp. 5206–5207, Nov 2016.

[14] A. D. Paquette and D. M. Divan, "Virtual impedance current limiting for inverters in microgrids with synchronous generators," *IEEE Trans. Ind. Appl.*, vol. 51, no. 2, pp. 1630–1638, 2015.

[15] J. W. Choi and S. C. Lee, "Antiwindup strategy for pi-type speed controller," *IEEE Trans. Ind. Electron.*, vol. 56, no. 6, pp. 2039–2046, June 2009.

[16] N. Bottrell and T. C. Green, "Comparison of current-limiting strategies during fault ride-through of inverters to prevent latch-up and wind-up," *IEEE Trans. Power Electron.*, vol. 29, no. 7, pp. 3786–3797, 2014.

[17] I. Sadeghkhani, M. E. H. Golshan, J. M. Guerrero, and A. Mehrizi-Sani, "A current limiting strategy to improve fault ride-through of inverter interfaced autonomous microgrids," *IEEE Transactions on Smart Grid*, vol. 8, no. 5, pp. 2138–2148, Sept 2017.

[18] X. Lu, J. Wang, J. M. Guerrero, and D. Zhao, "Virtual-impedance-based fault current limiters for inverter dominated ac microgrids," *IEEE Transactions on Smart Grid*, vol. 9, no. 3, pp. 1599–1612, May 2018.

[19] Q. C. Zhong and G. C. Konstantopoulos, "Current-limiting droop control of grid-connected inverters," *IEEE Transactions on Industrial Electronics*, vol. 64, no. 7, pp. 5963–5973, July 2017.

[20] N. Pogaku, M. Prodanovic, and T. C. Green, "Modeling, analysis and testing of autonomous operation of an inverter-based microgrid," *IEEE Transactions on Power Electronics*, vol. 22, no. 2, pp. 613–625, March 2007.

[21] S. Golestan, J. M. Guerrero, and J. C. Vasquez, "A pll-based controller for three-phase grid-connected power converters," *IEEE Transactions on Power Electronics*, vol. 33, no. 2, pp. 911–916, Feb 2018.

[22] C. T. Rim, D. Y. Hu, and G. H. Cho, "Transformers as equivalent circuits for switches: general proofs and d-q transformation-based analyses," *IEEE Transactions on Industry Applications*, vol. 26, no. 4, pp. 777–785, Jul 1990.

[23] Q.-C. Zhong and T. Hornik, *Control of Power Inverters in Renewable Energy and Smart Grid Integration*. New York, NY, USA: Wiley-IEEE Press, 2013.

[24] B. K. Bose, *Modern Power Electronics and AC Drives*. Prentice Hall PTR, 2002.

[25] Q. C. Zhong and G. C. Konstantopoulos, "Current-limiting three-phase rectifiers," *IEEE Transactions on Industrial Electronics*, vol. 65, no. 2, pp. 957–967, Feb 2018.

[26] R. Teodorescu, M. Liserre, and P. Rodriguez, *Grid Converters for Photovoltaic and Wind Power Systems*. John Wiley & Sons, LTD, 2011.

[27] G. C. Konstantopoulos, Q. C. Zhong, B. Ren, and M. Krstic, "Bounded integral control of input-to-state practically stable nonlinear systems to guarantee closed-loop stability," *IEEE Transactions on Automatic Control*, vol. 61, no. 12, pp. 4196–4202, Dec 2016.